

# We are IntechOpen, the world's leading publisher of Open Access books Built by scientists, for scientists

6,900

Open access books available

186,000

International authors and editors

200M

Downloads

Our authors are among the

154

Countries delivered to

TOP 1%

most cited scientists

12.2%

Contributors from top 500 universities



WEB OF SCIENCE™

Selection of our books indexed in the Book Citation Index  
in Web of Science™ Core Collection (BKCI)

Interested in publishing with us?  
Contact [book.department@intechopen.com](mailto:book.department@intechopen.com)

Numbers displayed above are based on latest data collected.  
For more information visit [www.intechopen.com](http://www.intechopen.com)



# Numerical simulation of a semi-active vibration control device based on superelastic shape memory alloy wires

Corneliu Cismaşiu and Filipe P. Amarante dos Santos

*Centro de Investigação em Estruturas e Construção - UNIC, Faculdade de Ciências e Tecnologia, Universidade Nova de Lisboa, 2829-516 Caparica Portugal*

## 1. Introduction

The martensitic transformations exhibited by shape memory alloys (SMAs) are diffusionless phase transformations in solids, that change the material from the parent phase, a cubic crystal structure called austenite, to a lower symmetry monoclinic crystal structure, called martensite. These phase transformations yield the shape memory effect and superelasticity, peculiar thermo-mechanical properties which make the SMAs very appealing for applications in Civil Engineering structures.

Superelasticity allows the material to recover from large nonlinear strains during a mechanical cycle of loading and unloading, while dissipating a considerable amount of energy through hysteresis. The chemical composition of the alloy, as well as its thermomechanical treatment, has an important influence on the SMA properties and on the extent of the area enclosed by the hysteretic loop (Ortín & Delaey, 2002; Otsuka & Wayman, 1998).

Exploiting this property, several authors report on successful implementations of SMAs in passive vibration control devices. Most of them are especially designed for seismic hazard mitigation. They range from simple austenitic superelastic (SE) wires in bracing systems (Torra et al., 2007) to hinge restrainers SE bars in bridges (DesRoches & Delemont, 2002). A combination of martensitic bars or austenitic SE wires with pre-stressed SE wires working in phase opposition have also been successfully implemented both in bracing and isolation systems (Dolce et al., 2000; 2005). Additionally, steel beam to column connections, built up of martensitic bars, have also been reported (Ocel et al., 2004). Most of these devices are built up of Nitinol (NiTi), a dual alloy built up of Nickel and Titanium (Zhang & Zu, 2007), due to its outstanding fatigue properties, high corrosion resistance and ductility. A hybrid base isolation system, composed of linear elastomeric bearings, friction-pendulum bearings, SE austenitic wires and magnetorheological dampers was proposed by Shook *et al.* (Shook et al., 2008) for mitigation of seismic motions. To manage the superstructure response to ground motions, each subcomponent of the isolation system was designed for a specific task. The SE austenitic wires were used to supply recoverable hysteretic behavior and to serve as an additional restoring force. Zhang and Zu (Zhang & Zu, 2007) propose an adaptive vibration control device based on SE austenitic wires that presents two distinctive features: its tunable

hysteretic behavior and the ability to withstand several design level earthquakes. The hysteretic behavior of the damper could be modified to best fit passive structural control applications by adjusting dampers design parameters such as the inclination angle of the SE wires, pre-tension level and the friction coefficient.

The vibration control device proposed in the present work, originates from the NiTi based passive dissipation device reported by Dolce *et al.* (Dolce *et al.*, 2000). As to increase its energy dissipation capabilities, the original device was made of sets of pretensioned wires working in phase opposition. However, a variety of relaxation phenomena observed in pretensioned SE wires (Bhattacharyya *et al.*, 2002; Matsui *et al.*, 2004) might have an adverse impact on the dynamic performances of the device. Mainly to avoid these problems, the proposed semi-active device uses a strategy that allows the continuous adapting of the accumulated strain in the wires, based on the response of the device to external excitations. As in an active control system, a controller monitors the feedback measurements and generates appropriate command signals for the device. As in a passive control system however, the control forces are developed as a result of the motion of the structure itself, with no need of external energy input. As the control forces act as to oppose the motion of the structural system, they promote the global stability of the structure (Symans & Constantinou, 1999). According to presently accepted definitions (Housner *et al.*, 1997), the proposed device may be considered as a semi-active control system.

## 2. Thermo-mechanical properties

While some other commercial forms are also available, namely tubes, strips and sheets, NiTi is most commonly used in form of wire or bars. In order to characterize its tensile behavior in wire form, three sets of experimental tests were performed on NiTi SE508 wire specimens, with 2.4 mm diameter and circular cross section, provided by Euroflex GmbH.

### 2.1 DSC thermo-analytical analysis

In the stress-free state, a SMA is characterized by four transformation temperatures:  $M_s$  and  $M_f$  during cooling and  $A_s$  and  $A_f$  during heating. The first two (with  $M_s > M_f$ ) indicate the temperatures at which the forward transformation starts and finishes, respectively. The last two (with  $A_s < A_f$ ) are the starting and finishing temperatures for the inverse transformation. One of the most used methods to identify these transformation temperatures, is the Differential Scanning Calorimetry (DSC) (Höhne *et al.*, 2003), a thermo-analytical technique in which the difference in the amount of heat required to increase the temperature of a sample and a reference of well defined heat capacity, are measured as a function of temperature. Both the sample and the reference are maintained at nearly the same temperature throughout the experiment. The basic principle underlying this technique is that, when the sample undergoes physical transformations such as phase transitions, a different quantity of heat is needed to maintain it at the same temperature as the reference. If it's more or less, depends on whether the process is exothermic, as the forward martensitic transformation, or endothermic, as the inverse martensitic transformation. Care must be taken as the presence of an eventual R-phase prior to thermal cycling and residual stresses from sample cutting tends to complicate the curves and introduce spurious peaks (Collings, 1995). In order to characterize the transformation temperatures of the SE NiTi SE508 wire specimen, a DSC test was performed using a SETARAM-DSC92 thermal analyzer, Figure 1(a). Although the sample was tested as received, prior to the DSC analysis it was submitted to a chemical etching in order to remove

the oxide and the layer deformed by the cutting operation. During the DSC analysis, the sample was heated up to 80°C, held at this temperature for 6 min and then cooled to -80°C, with heating/cooling rates of 7.5°C/min. A baseline analysis of the resulting curves is presented in Figure 1(b), where the four transformation temperatures can be easily identified. Their values are presented in Table 1.

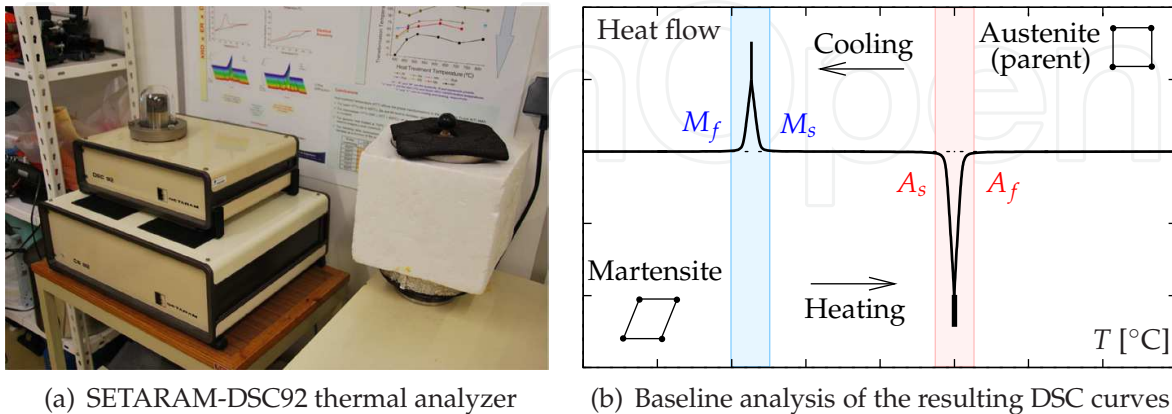


Fig. 1. Differential Scanning Calorimetry thermo-analytical analysis

### 2.2 Quasi-static tensile tests at room temperature

To complete the material characterization, the SE NiTi SE508 wire specimen was also subjected to a pseudo-static, strain driven uniaxial tensile test on a Zwick/Roell Z050 testing machine, Figure 2(a), with a strain rate of 0.02%/s. The tests were conducted at a room temperature of 24°C up to a maximum strain of 6%.

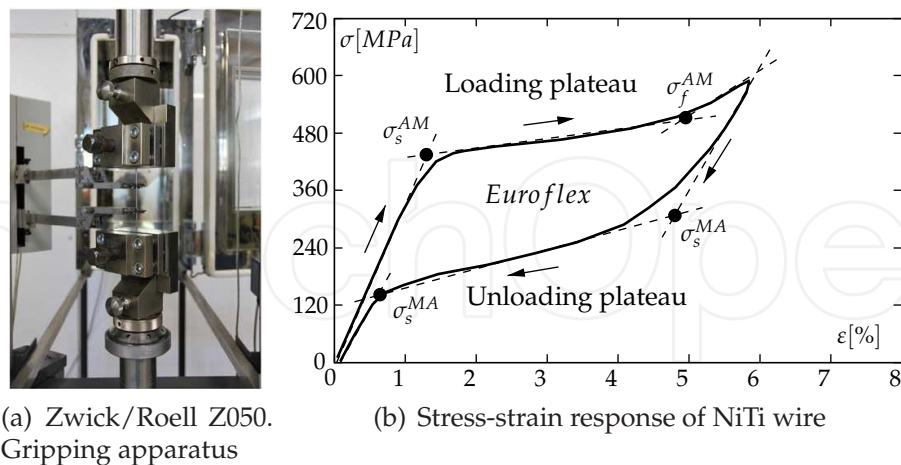


Fig. 2. Quasi-static uniaxial tensile test

The usual shape of a superelastic hysteric cycle, characterized by two regions of almost constant stress, the loading and the unloading plateaux during the forward and inverse transformations, is clearly captured, as illustrated in Figure 2(b). Based on the inspection of this

resulting stress-strain response, the austenitic and martensitic elastic modulus (Auricchio & Sacco, 1997), the maximum residual strain, as well as the starting and final stresses during the forward and inverse transformation, are identified and collected in Table 1. For the Poisson's ratio, a typical value of 0.33 is adopted from the literature (Collings, 1995).

### 2.3 Quasi-static tensile tests at different ambient temperatures

Another parameter needed in the definition of the constitutive model is the Clausis-Clapeyron coefficient (CCC), representing the slope ( $d\sigma/dT$ ) of the lines defining the boundaries of the SMA transformation strips in the material's phase plane diagram, Figure 6(a). Note that, the CCC is assumed to be the same for the forward,  $C_M$  and inverse,  $C_A$ , transformations.

According to (Isalgue et al., 2008), the most straightforward experimental procedure to compute the CCC of a previously stabilized SMA specimen is to determine its critical transformation stresses for a set of different ambient temperatures. Based on this principle, an experimental testing procedure was implemented and conducted using a Zwick/Roell Z050 testing machine and a W91255 temperature controlled chamber, Figure 3.

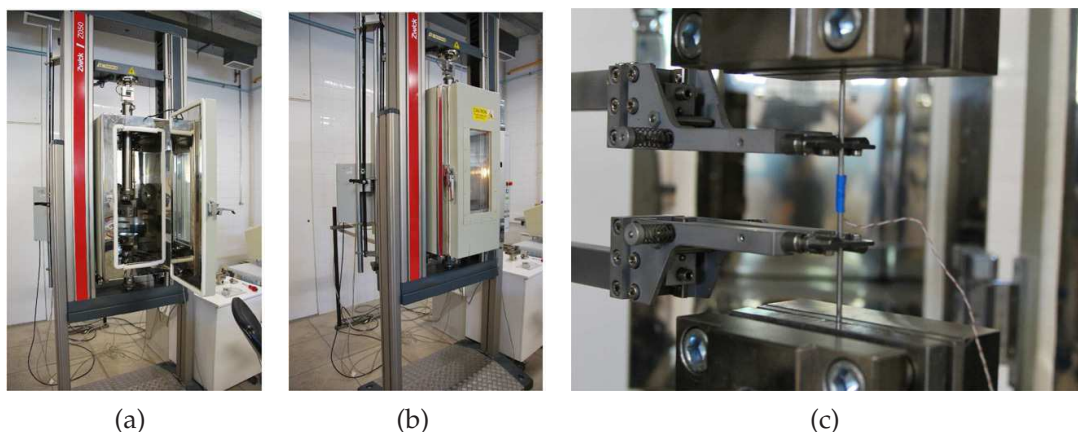


Fig. 3. W91255 temperature controlled chamber (a) prior and (b) during the temperature controlled tensile testing and (c) detail of the thermocouple

The SE NiTi SE508 wire specimen was strained up to 7.5% with a strain rate of 0.068%/s, in an ambient temperature that ranged from 30 to 78°C, with an increment of 3°C. The temperature in the wire was constantly monitored by a thermocouple placed at its mid section.

The resulting stress-strain curves are displayed in Figure 4(a). Observing these graphs, it is clear that the superelastic hysteresis shifts upwards as the ambient temperature rises. In order to estimate the CCC, the stress variation with temperature must be evaluated. As particular hysteretic points, like, for instance, the one associated with the beginning of the forward transformation, may be difficult to identify, the average variation of the stress on the loading plateau was used. For the prescribed temperature increment, its value was 19.5 MPa, leading to a CCC of 6.5 MPaK<sup>-1</sup>. Experimental results reported in the literature (Isalgue et al., 2008) present similar CCC values, 6.6±0.2 MPaK<sup>-1</sup>, in a NiTi wire specimen with 2.46 mm diameter. The plot in Figure 4(b), represent the linear relation between temperature and the stress

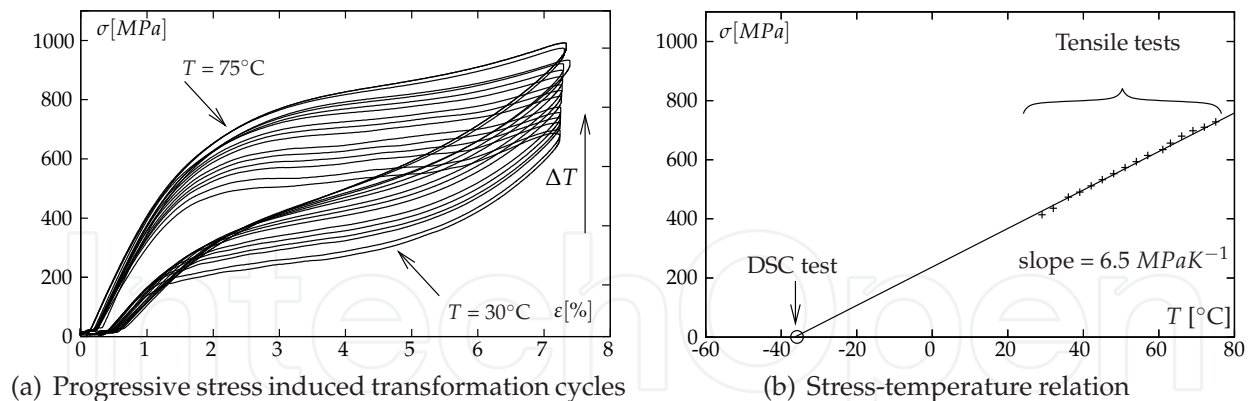


Fig. 4. Temperature dependence of the stress induced martensitic transformation in quasi-static uniaxial tensile tests

associated with the beginning of the forward transformation, and it was obtained using the estimated for the CCC and the  $M_s$  value from the DSC analysis.

### 3. Constitutive model

The behavior of SMAs denotes a high level of complexity, as it depends on stress and temperature and is closely connected with the crystallographic phase of the material and the thermodynamics underlying the transformation processes. For this reason, any simulation regarding the design of a particular system that exploit the interesting features exhibited by these materials, must be based on an adequate constitutive model. The model must be able to conveniently cope with the relevant set of SMA's properties regarding the type of application at stake. While strain or stress rate independent models (Auricchio et al., 2006; 1997; McCormick et al., 2006), may be well suited for quasi-static analysis when isothermal conditions may be assumed, for most dynamic applications, rate dependent models are usually required, due to self-heating (Ivshin & Pence, 1994; Liang & Rogers, 1990; Tanaka et al., 1986).

Several constitutive mathematical models are currently available in the literature, most of them being aimed at the one-dimensional description of the material behavior (Auricchio & Sacco, 1997; Brinson & Huang, 1996; Liang & Rogers, 1990). One of the common features present in most of them, is the presence of a distinct mechanical law, governing the stress-strain relations, and of a kinetic law, governing the martensitic transformations. In the case of rate dependent models, to conveniently model the thermal effects, a heat balance equation is coupled with the mechanical and kinetic transformation laws.

#### 3.1 Mechanical laws

In a typical SMA constitutive model, the mechanical law relates the stress ( $\sigma$ ), strain ( $\epsilon$ ), temperature ( $T$ ) and martensite fraction ( $\zeta$ ). The martensite fraction is an internal state variable, representing the extent of the transformation in the material and can be regarded as the fraction of the produced phase. This transformed phase fraction is considered to be in series with the elastic fraction. According to the literature (Brinson & Huang, 1996), there are several possible approaches to model the elastic component. If considered to be limited to the austenitic

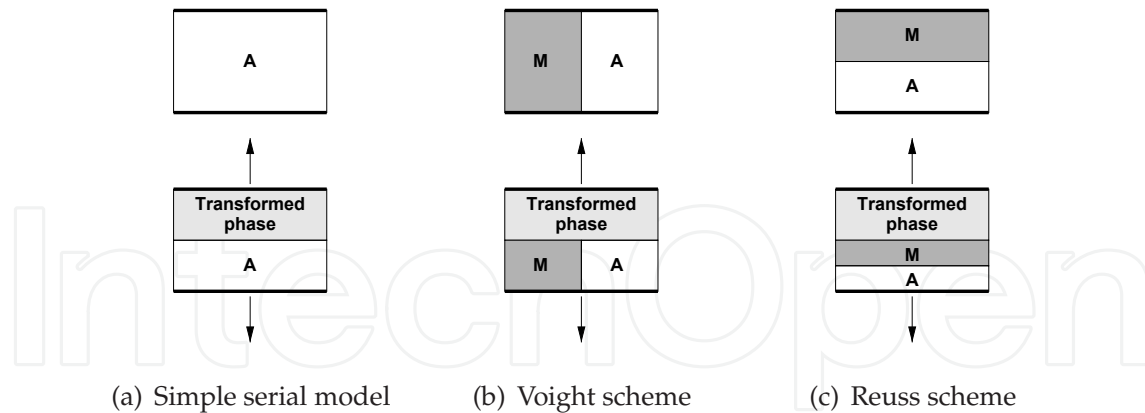


Fig. 5. SMA's mechanical laws

phase, the simple serial model presented in Figure 5(a) is obtained. If, however, two crystallographic phases, the austenite and martensite<sup>1</sup> are to be contemplated in this elastic phase, two cases can be considered, namely the Voigt and the Reuss schemes. The Voigt scheme, Figure 5(b), considers a parallel distribution of austenite and martensite within the material, while the Reuss scheme, Figure 5(c) is based on the assumption of a periodical distribution of austenite and martensite within the material, orthogonal to the direction of the applied stress.

### 3.1.1 Simple serial model

In the case of the simple serial model illustrated in Figure 5(a), as the principle of superposition applies, the total strain yields adding the elastic  $\varepsilon_{elast.}$  to the transformation strain  $\varepsilon_{transf.}$

$$\varepsilon = \varepsilon_{elast.} + \varepsilon_{transf.}$$

Knowing that the transformation strain can be expressed function of the maximum residual strain in the material,  $\varepsilon_L$ , and the martensite fraction as  $\varepsilon_L \zeta$ , and taking into account that the elastic strain equals the austenitic strain,  $\varepsilon_A$ , the total strain reads

$$\varepsilon = \varepsilon_A + \varepsilon_L \zeta \quad \text{with} \quad 0 \leq \zeta \leq 1$$

and the mechanical law relating the strains and the stresses yields

$$\sigma = \sigma_A = E_A \varepsilon_A = E_A (\varepsilon - \varepsilon_L \zeta)$$

where  $E_A$  is the austenitic elastic modulus. The model neglects the additional thermal strain component, which is several orders of magnitude smaller than the transformation strain (Brinson & Huang, 1996).

### 3.1.2 Voigt scheme

In the Voigt scheme, as clearly illustrated in Figure 5(b), the elastic, austenitic and martensitic strains are all equal and therefore, the mechanical law governing the material behavior can be written as

$$\sigma = \zeta \sigma_M + (1 - \zeta) \sigma_A$$

<sup>1</sup> Not distinguishing between the twinned and the detwinned martensite.

Using the definition for the austenitic and martensitic stresses,  $\sigma_A = E_A \varepsilon_A$  and  $\sigma_M = E_M \varepsilon_M$ , the mechanical law can be expressed as

$$\sigma = [\zeta E_M + (1 - \zeta) E_A] (\varepsilon - \varepsilon_L \zeta)$$

where  $\varepsilon_M$  and  $E_M$  are the martensitic strain and elastic modulus, respectively. Adding a thermal strain component to the above result, yields the mechanical law proposed by Tanaka (Tanaka et al., 1986),

$$\sigma = [\zeta E_M + (1 - \zeta) E_A] (\varepsilon - \varepsilon_L \zeta) + \theta(T - T_0)$$

where  $\theta$  is the thermal coefficient of expansion and  $T_0$  the temperature at which the thermal strain is defined to be zero.

### 3.1.3 Reuss scheme

In the Reuss scheme, and according to Figure 5(c), it can be seen that the total strain can be expressed as

$$\varepsilon = \zeta \varepsilon_M + (1 - \zeta) \varepsilon_A$$

Taking into account that the stress in each phase is equal to the overall applied stress and using the definition of the austenitic and martensitic strains,  $\varepsilon_A = \sigma/E_A$  and  $\varepsilon_M = \sigma/E_M + \varepsilon_L$ , the mechanical law can be expressed as

$$\sigma = \frac{E_A E_M}{\zeta E_A + (1 - \zeta) E_M} (\varepsilon - \varepsilon_L \zeta)$$

The Ivshin-Pence mechanical law (Ivshin & Pence, 1994) can be recovered by adding the thermal strain component to the above equation, to read,

$$\sigma = \frac{E_A E_M}{\zeta E_A + (1 - \zeta) E_M} (\varepsilon - \varepsilon_L \zeta) + \theta(T - T_0)$$

## 3.2 Kinetic laws

The transformation kinetic laws describe mathematically the evolution of the martensite fraction with stress and temperature, based on the material's stress-temperature phase diagram. Several kinetic laws are available in the literature, ranging from linear (Auricchio & Sacco, 1997) or exponential laws (Tanaka et al., 1986), to cosine based kinetic laws (Liang & Rogers, 1990) and thermodynamically derived relations (Ivshin & Pence, 1994).

The linear and the exponential kinetic laws are briefly described in what follows.

### 3.2.1 Linear transformation kinetic law

The linear transformation kinetic laws are based on the assumption that the relation between strains and stresses are represented by a series of linear segments. The material constants,  $M_f$ ,  $M_s$ ,  $A_s$ ,  $A_f$ ,  $C_M$  and  $C_A$ , are illustrated in the stress-temperature phase diagram in Figure 6(a), where an isothermal, stress induced martensitic transformation path is drawn. The starting and final stresses during the forward,  $\sigma_s^{AM}$  and  $\sigma_f^{AM}$ , and inverse transformations,  $\sigma_s^{MA}$  and  $\sigma_f^{MA}$ , are represented in the corresponding strain-stress diagram. As the scalar variable  $\zeta$  represents the martensite fraction during the phase transformation, its variation occurs during the conversion of austenite into martensite ( $A \rightarrow M$ ) or of martensite into austenite ( $M \rightarrow A$ ),

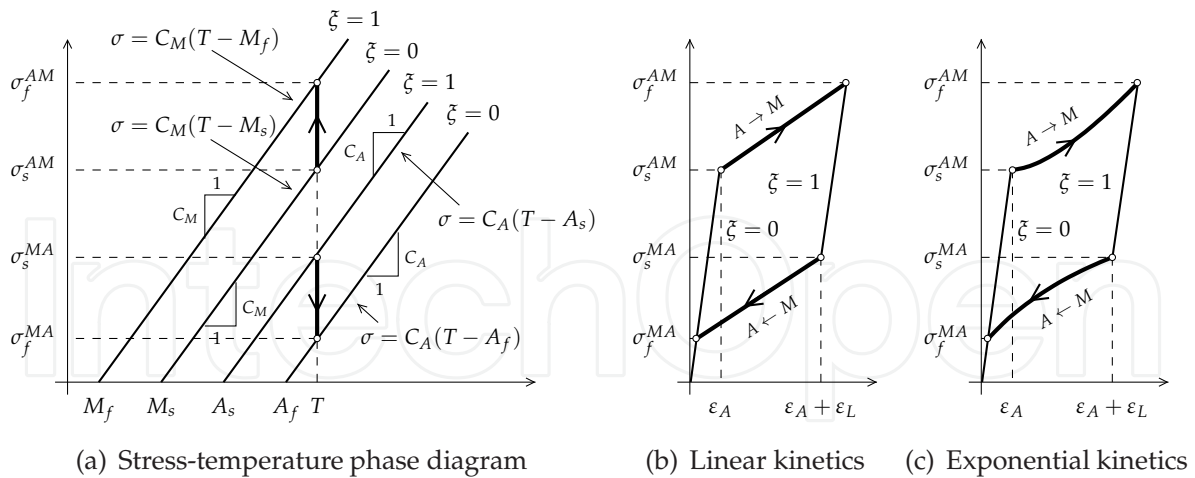


Fig. 6. Phase diagram and transformation kinetics

the forward and inverse transformations, respectively. In the case of linear kinetics, the function  $\xi(\sigma)$  presents a linear behavior, assuming values between zero and one, corresponding to the pure austenite and martensite phases. Hence, for a specific temperature,  $T$ , the kinetic laws describing the forward and inverse transformations can be expressed as

$$\xi^{AM} = \frac{\sigma - \sigma_s^{AM}}{\sigma_f^{AM} - \sigma_s^{AM}} \quad \xi^{MA} = \frac{\sigma - \sigma_f^{MA}}{\sigma_s^{MA} - \sigma_f^{MA}}$$

The equations defining the boundary lines of the transformation strips represented in Figure 6(a) are introduced in the equations above to yield the linear kinetic laws for the forward and inverse transformations, respectively,

$$\xi^{AM} = \frac{\sigma - C_M(T - M_s)}{C_M(M_s - M_f)} \quad \xi^{MA} = \frac{\sigma - C_A(T - A_f)}{C_A(A_f - A_s)}$$

### 3.2.2 Exponential transformation kinetic law

The exponential kinetic laws are based on the Magee's equations, originally proposed for steels (Magee, 1970). For the forward and inverse transformations, they yield,

$$\frac{\dot{\xi}^{AM}}{1 - \xi^{AM}} = a_M \dot{T} - b_M \dot{\sigma} \quad - \frac{\dot{\xi}^{MA}}{\xi^{MA}} = a_A \dot{T} - b_A \dot{\sigma}$$

The well known (Vitiello et al., 2005) exponential kinetic laws results by integrating the above equations from the initial values  $(\sigma_0, T_0, \xi_0)$  to the current values  $(\sigma, T, \xi)$ , for constant material parameters  $a_M, b_M, a_A$  and  $b_A$  and taking into account that  $b_M C_M = a_M$  and  $b_A C_A = a_A$ , to yield, for the forward and inverse transformations,

$$\xi^{AM} = 1 - \exp [a_M(M_s - T) + b_M \sigma] \quad \xi^{MA} = \exp [a_A(A_s - T) + b_A \sigma]$$

To determine the material constants  $a_M$  and  $b_M$ , one follows the usual understanding in metallurgy (Jones & Ashby, 1998), assuming that the forward transformation is complete when

$\zeta = 0.99$ . The material constants  $a_A$  and  $b_A$  are calculated in a similar way, assuming that the inverse transformation is complete when  $\zeta = 0.01$ . Using these assumptions, simple algebraic manipulations yield,

$$a_M = -\frac{2 \ln 10}{M_s - M_f} \quad b_M = \frac{a_M}{C_M} \quad a_A = \frac{2 \ln 10}{A_f - A_s} \quad b_A = \frac{a_A}{C_A}$$

### 3.3 Heat balance equation

When quasi-static loading conditions can be assumed, the heat exchanges between the superelastic material and its surrounding environment generate almost isothermic processes. However, as the rate of dynamic loading increases, since the dissipation capacity of the thermo-mechanical system is limited by the heat convection mechanism, the generated and the dissipated energy become unbalanced, causing changes in the specimen's temperature and shape of the hysteric loop, and consequently, in the damping capacity of the material itself. In order to attend this phenomena, whilst modeling the dynamical behavior of these materials, the mechanical and kinetic laws must be coupled with a heat balance equation considering the thermal effects on the material (Cismasiu & Santos, 2008; Koistinen & Marburger, 1959; Vitiello et al., 2005).

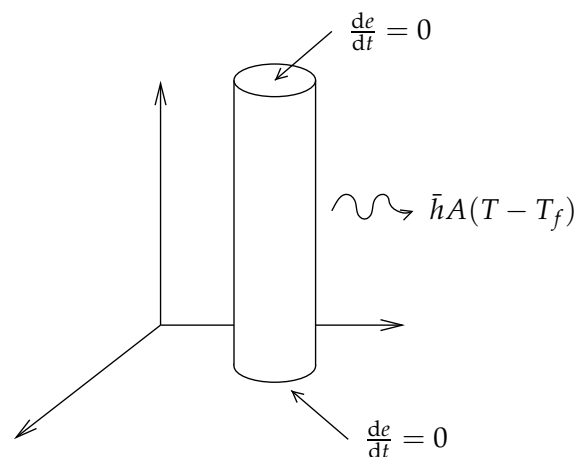


Fig. 7. Heat transfer system

The heat transfer system under analysis, presented in Figure 7, consists of a superelastic NiTi wire with circular cross section, fixed at both ends and surrounded by air, at temperature  $T_f$ . There are internal energy sources within the wire, deriving from the enthalpy of the martensitic transformations and internal friction, both occurring during a hysteretic superelastic cycle. It is assumed that the heat conduction through the wire's extremities is negligible and therefore, it is possible to consider only the lateral surface for calculating the heat exchanges with the environment. The conduction heat transfer phenomena is described by the Fourier's law (Holman, 2009),

$$q = -k\nabla T$$

in which the heat flux  $q$  is expressed as a function of the temperature profile and the thermal conductivity,  $k$ . The minus sign ensure that the heat flows downwards the temperature gradient. According to the conservation of energy, for a small element within the body, the

non-stationary conductive problem can be described by the differential equation of heat conduction with a generating term,

$$\nabla q = q_{gen} - \frac{de}{dt}$$

The power generated per unit of volume,  $q_{gen}$ , describes the rate of heat generation within the body. Typically, this new heat must be conducted to the boundaries and removed via convection and/or radiation heat transfer. The change in the internal energy,  $e$ , is related to the body's ability to store heat by raising its temperature, and can be expressed as

$$\frac{de}{dt} = \rho c \frac{dT}{dt}$$

where  $\rho$  is the density of the material and  $c$  its specific heat. The heat balance equation results substituting the Fourier's law and the definition of the change in the internal energy in the differential equation of the conduction of heat, to yield

$$\nabla^2 T - \frac{\rho c}{k} \frac{dT}{dt} = -\frac{q_{gen}}{k}$$

This equation can be reduced to a simpler form if one can assume a uniform temperature within the specimen, as, under such conditions, the temperature depends only on time. To check the applicability of the above assumption, one can compute the Biot number,  $Bi$ , a dimensionless value that gives a simple index of the ratio of the heat transfer resistance inside and at the surface of a body. This ratio determines whether or not the temperature inside a body will vary significantly in space, while the the body heats or cools over time. The Biot number is defined as

$$Bi = \frac{\bar{h}L_c}{k}$$

where  $L_c$  is the characteristic length, commonly defined as the volume of the body divided by its surface area,  $\bar{h}$  is the mean coefficient of heat transfer and  $k$  the thermal conductivity. Values of the Biot number less than 0.1 imply that the heat conduction inside the body is much faster than the heat convection away from its surface and therefore, the temperature gradients are negligible inside of it. In these cases, the use of a one-dimensional analysis leads to errors less than 10% (Holman, 2009) and the heat balance equation can be simplified to,

$$-\rho c V \frac{dT}{dt} = \bar{h} A (T - T_f) - q_{gen} V \quad \text{with} \quad T(0) = T_f$$

where  $V$  is the volume of the body and  $A$  its surface area. The power generated per volume unit, appearing in the above equation, is defined as,

$$q_{gen} = c_L \rho \frac{d\xi}{dt} + \frac{dW}{dt}$$

where the first term is related to the martensite fraction, assuming constant latent heat,  $c_L$ . The second is related to internal friction. As in a complete tensile loading-unloading cycle, the dissipated energy by internal friction,  $W$ , corresponds to the total area enclosed by the hysteretic loop, the associated power results dividing this area by the duration of the cycle.

### 3.4 Adopted constitutive model

The rate-dependent constitutive model used in the following numerical simulations is based on Tanaka's temperature dependent model (Tanaka et al., 1986). In order to relate stress, strain, temperature and martensite fraction in the material, the model couples the constitutive relations to an exponential kinetic law that describes the volume fraction of austenite (Koistinen & Marburger, 1959). When associated to a balance equation that considers the thermal effects on the material, this constitutive model produces reliable results even for high strain rates (Cismasiu & Santos, 2008; Vitiello et al., 2005).

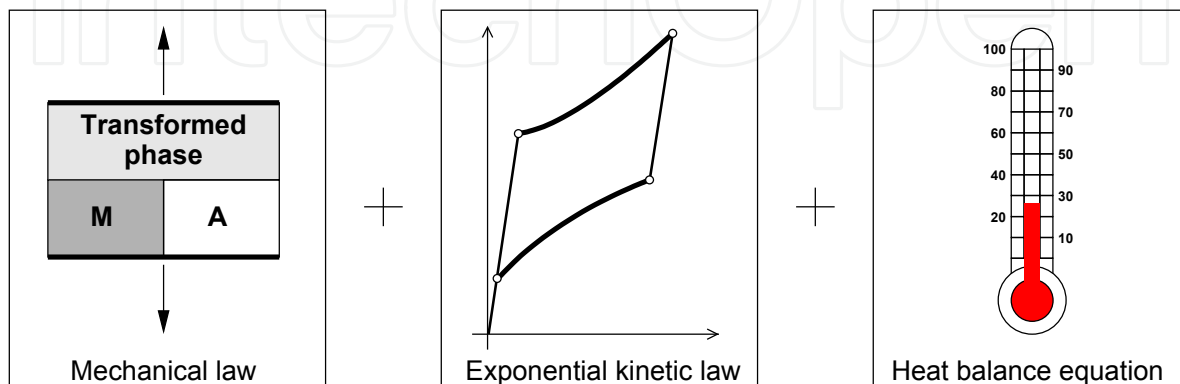


Fig. 8. Adopted constitutive model: Voight scheme, exponential kinetics and heat balance equation

The values reported in (Vitiello et al., 2005) for the following thermophysical properties: latent heat,  $c_L$ , specific heat,  $c_p$ , density,  $\rho$ , convection coefficient,  $h$  and thermal expansion coefficient,  $\theta$ , are used to complete the model characterization. All these parameters are presented in Table 1.

$E_A = 35000 \text{ MPa}$	$E_M = 20000 \text{ MPa}$	$M_f = -45^\circ \text{ C}$
$M_s = -35^\circ \text{ C}$	$A_s = -15^\circ \text{ C}$	$A_f = -5^\circ \text{ C}$
$C_M = 6.5 \text{ MPaK}^{-1}$	$C_A = 6.5 \text{ MPaK}^{-1}$	$e_L = 3\%$
$\rho = 6500 \text{ kg m}^{-3}$	$c_L = 12914 \text{ J kg}^{-1}$	$c_p = 500 \text{ J kg}^{-1}\text{K}^{-1}$
$h = 35 \text{ W m}^{-2} \text{ K}^{-1}$	$\theta = 6 \times 10^{-6} \text{ K}^{-1}$	$k = 18 \text{ W m}^{-2} \text{ K}^{-1}$

Table 1. Parameters for adopted constitutive model

### 3.5 Numerical assessment of the adopted constitutive model

The results of a large set of experimental cyclic tensile tests on 2.4 mm diameter NiTi S wires provided by *Euroflex GmbH*, clearly illustrating the sensitivity of the mechanical response to temperature and strain rate, are used to assess the performances of the constitutive model. All tests were conducted on a Zwick/Roell Z050 testing machine, equipped with a W91255 temperature controlled chamber, Figures 2(a) and 3.

### 3.5.1 Quasi-static tensile tests

To start with, the experimental curves obtained from a set of quasi-static tensile tests, carried out at a strain rate of 0.020%/s in an ambient temperature of 24°C, were compared with the numerical model estimates. As is illustrated in Figure 9(a) and 9(b), for the case of three complete cycles of decreasing amplitude and for the case of a complete cycle followed by a smaller inner cycle, the model is able to describe a wide variety of loading histories, with numerical predictions that fit well the experimental data. Particularly good estimates are obtained dur-

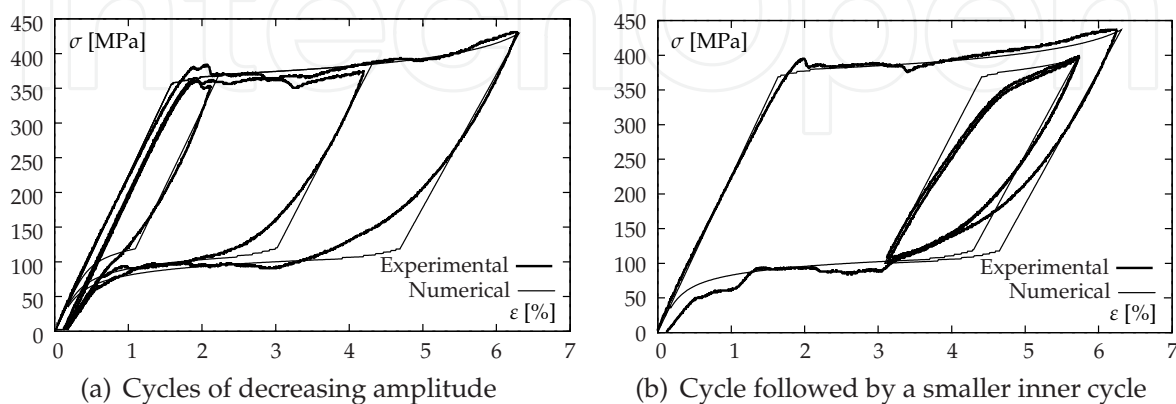


Fig. 9. Quasi-static experimental tests: numerical model versus experimental data

ing the forward transformation, when the relative error between the experimental data and the numerical simulation is practically negligible. However, upon unloading, apart from the initial segment, where the stiffness is accurately captures, the model seems to overestimate the SMA's stiffness. This can be explained by the fact that the constitutive model does not capture the gradual transition to the inverse transformation plateau.

### 3.5.2 Dynamic tensile tests

The ability of the adopted constitutive model to conveniently model the complex thermo-mechanical response of the superelastic NiTi wire during dynamic loading is investigated next. The experimental curves obtained in four tensile tests, carried out at different strain rates,  $\dot{\epsilon} = 0.008, 0.067, 0.250$  and  $0.333\%/s$ , in an ambient temperature of 20°C, are compared with the simulated estimates. The plots in Figure 10 clearly illustrate that the implemented rate-dependent numerical model yields a set of very satisfying results, both for the temperature time histories and their corresponding stress-strain diagrams. It can be seen that, as the strain rate of the dynamic loading increases from 0.008 to 0.333%/s, the simulation predicts increasing changes in the sample temperature during the loading cycle, in close agreement with the experimental data. In what concern the stress-strain diagram, the shape of the hysteretic loops tends to become steeper and narrower with the increase in the strain rate, again in conformity with the trend observed in the experimental tests.

## 4. Proposed semi-active vibration control device under harmonic excitation

The proposed semi-active control device, whose generic functional scheme is given in Figure 11(b), is based on the passive system illustrated in Figure 11(a), being built up of two SE wires working in phase opposition. In passive systems of this type, the wires are connected to

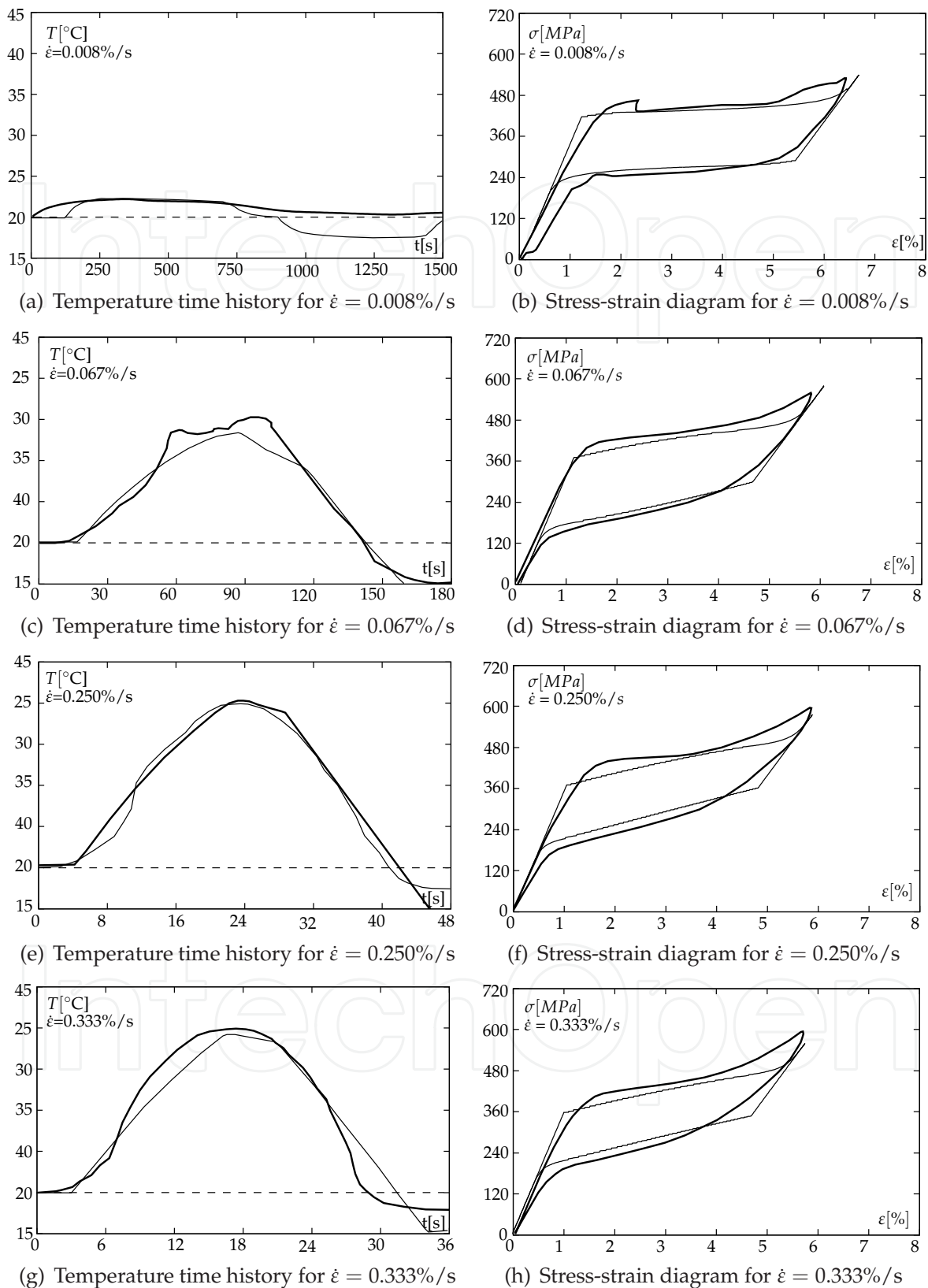


Fig. 10. Dynamic experimental tests at ambient temperature of 20°C: numerical model versus experimental data

the mass,  $m$ , and act as restoring elements. During the loading cycles, while one of the wires is loaded the other one is unloaded and conversely (Cismasiu & Santos, 2008; Dolce et al., 2000; 2005).

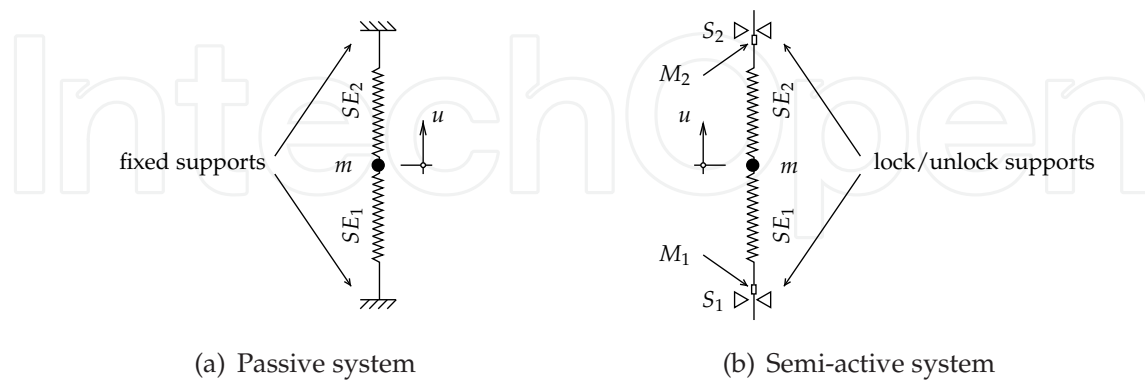


Fig. 11. Generic functional scheme of the passive and the semi-active systems: superelastic wires ( $SE_1$  and  $SE_2$ ), supports ( $S_1$  and  $S_2$ ) and markers ( $M_1$  and  $M_2$ )

The response of a passive vibration system, with and without pre-strain, to harmonic ground accelerations is recalled, to emphasize their dynamic characteristics. Their drawbacks are identified and used as conditioning design parameters for the proposed semi-active system. In the numerical simulations that follows, the system, with zero initial conditions, is excited during 1 second by a 2 Hz harmonic ground acceleration with an amplitude of  $1.25 \text{ ms}^{-2}$ . The analyses consider also a sequential phase of free oscillations. In all these numerical tests, the nonlinear equation of motion is solved using a Newmark predictor-corrector implicit algorithm (Chopra, 2001), implemented in a specially designed numerical framework (Cismasiu & Santos, 2008).

#### 4.1 Passive system with no pre-strain

The generic functional scheme of such a passive system, with the two superelastic elements,  $SE_1$  and  $SE_2$ , each one composed by 10 NiTi wires with a length of 1000 mm and 0.24 mm diameter, is given in Figure 11(a). The mass of the system is 100 kg and the SMA's material parameters are the ones in Table 1. Its strain and displacement time history responses to the prescribed harmonic excitation are presented in Figure 12. Facing compression, the wires exhibit zero stiffness and therefore  $SE_1$  and  $SE_2$  work alternately, as can be observed in Figure 12(a). In this particular case, the extent of the martensitic transformation caused by the dynamic displacements of the mass is quite small, corresponding to a martensite transformation ratio of about 15 % and, hence, little damping occurs. The beginning of the martensitic transformation is represented in Figure 12(a) by the horizontal dot line,  $\varepsilon_{Ms} \simeq 1.25\%$ .

#### 4.2 Passive system with pre-strain

A common technique to enhance the damping capability of the system is to enforce a pre-strain in the SE wires (Dolce et al., 2000). For a given dynamic action, the value of the pre-strain can be computed as to guarantee that the wires will always be in tension and therefore, one

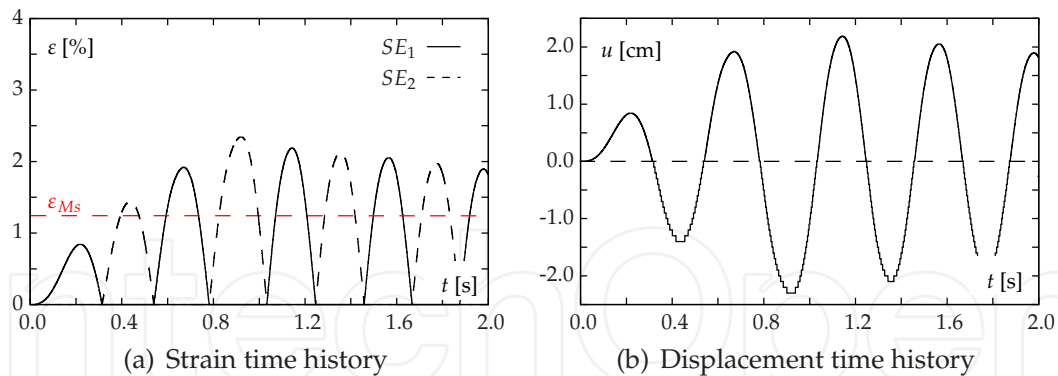


Fig. 12. Passive system with no pre-strain subjected to an harmonic load

can count with the contribution of both wires during the whole dynamic process. Moreover, one can set the initial strain to a level that can easily enable higher martensite transformation ratios and hence, higher damping (Zhang & Zu, 2007).

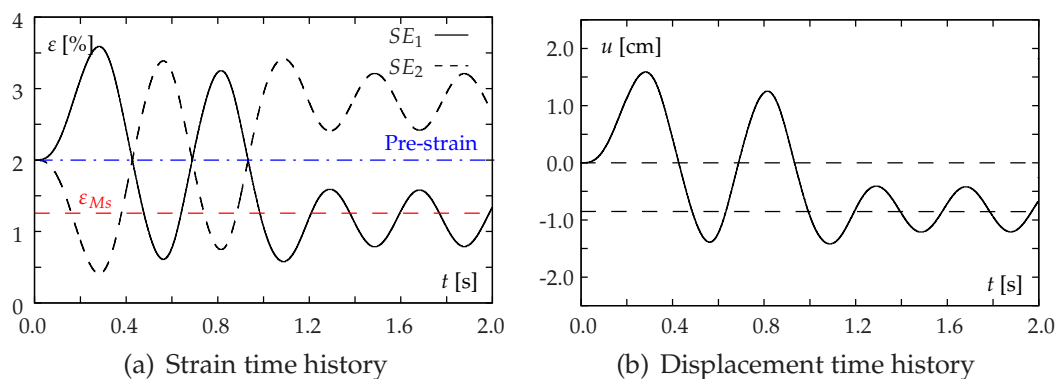


Fig. 13. Passive system with pre-strain subjected to an harmonic load

The effect of a 2.0% pre-strain in the wires of the previous passive system is illustrated in Figure 13, considering the same harmonic excitation. In this case, both of the SE wires are always active and they develop further martensitic transformation up to values of about 40 % martensite transformation ratio, meaning that the system is taking better advantage of the material's damping capabilities. However, two important drawbacks can be identified. First, this particular wire arrangement, with two pre-strained SE wires working in phase opposition, leads to a system with no recentering capability (Dolce et al., 2000). This can be confirmed in the displacements time history, during the steady state free vibration phase, when the oscillations are no longer centered in the original equilibrium position. The second, no less important drawback, relates to a variety of stress time effects that have been observed in various SMAs, that tend to adversely impact technological applications based on permanent pre-strained SE wires. According to the work presented by Auguet *et al.* (Auguet et al., 2008), in case of loading under stress controlled conditions, in the coexistence zone, stress seems to decrease under

constant strain. The fact that pre-stress gradually fades away with time becomes a major limitation of this type of devices for seismic applications.

Another phenomenon that might hinder the use of pre-strained SE wires in passive dissipation devices is the possible occurrence of permanent deformation due to cumulative SMA creep (Torra et al., 2007). When this happens, the length of the SE wire increases continuously with cycling, meaning that, for a given amplitude of the oscillations, the strain is reduced, along with the amount of dissipated mechanical energy. Cumulative creep in NiTi is linked with the introduction of dislocations and other lattice defects generated at high stress, during the preceding loading cycle (Miyazaki et al., 1986; Moumni et al., 2005). Hence, this accumulated deformation may be controlled by keeping the SE wire inside the recoverable limits of a so called pseudo-elastic window (PEW). These limits, which ensure an appropriate material behavior, are determined by the material composition and its thermo-mechanical treatment. In fact, the stability of the deformation behavior may be improved by raising the critical slip stress. Thermomechanical heat treatments aimed to stabilize the superelastic behavior of NiTi have been found effective (Miyazaki et al., 1986), minimizing cumulative creep and avoiding the modification of the hysteretic cycle.

While a simple solution, involving a third elastic element, exists in order to recover the re-centering capability of the system (Dolce et al., 2000; 2005), the remaining problems related to stress time effects and cumulative creep do not have a simple solution in a passive device configuration. Stress time effects can not be avoided, as the use of permanent pre-strained SE wires is a must in order to obtain competitive damping ratios. In what concerns the cumulative creep, keeping the strains inside the PEW is a very challenging task when dealing with arbitrary seismic excitation.

### 4.3 Semi-active system

The proposed semi-active control device minimizes the SMA rheological effects by controlling the strain in the SE wires. The strain is self-adjusting, allowing the wires to become strain/stress free, when not subjected to a dynamic excitation. The system is also able to keep the wires deformation inside a given PEW, while guaranteeing a minimal threshold to their strain level. The strain in the SE wires is calibrated by controlling the displacements of the wires at their supports. The two wire supports can assume, independently, two configurations, locked or unlocked. By default, the supports are locked, assuring the adequate restraining for the SE wires. If the system needs to compensate for an excessively low or high strain in a given wire, it momentarily unlocks the wire through a controlled velocity action and without introducing additional forces into the system. As the actuating elements only have two fixed positions, this type of control system is usually referred to as a two-position or on-off controller.

Each of the two SE wires is independently controlled. The output signal from the controller associated with the SE wire  $i$  is defined as  $U_i(s)$ . Each controller has two reference inputs,  $R_i^U(s)$  and  $R_i^L(s)$  corresponding to the strain upper and lower bound limits, which, in this case, are constants. The controlled process is defined by the transfer function  $G_{cpi}(s)$ . The output  $C_i(s)$  is fed back to the summing points, where it is compared with the reference inputs  $R_i^U(s)$  and  $R_i^L(s)$ , yielding the actuating error signals  $E_i^U(s) = R_i^U(s) - C_i(s)$  and  $E_i^L(s) = R_i^L(s) - C_i(s)$ . There is no need for a feedback-path transfer functions, to modify the output in order to make it comparable with the reference input signals, since the output of the numerical

simulation directly yields the updated strain value for each SE wire. The block diagram of the on-off control system for one SE wire is presented in Figure 14(a). The signal  $u_i(t)$  may

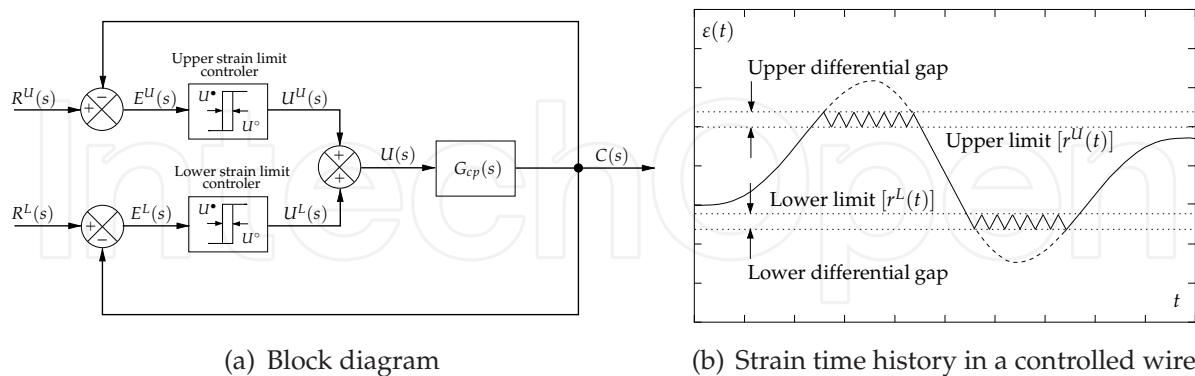


Fig. 14. On-off control system

assume the values  $U_i^*$  and  $U_i^o$ , corresponding to the locked and unlocked configurations of the SE wire's supports, so that

$$\begin{aligned}
 u_i(t) &= U_i^* \text{ (locked), for } e_i^U(t) > 0 \text{ or } e_i^L(t) < 0 \\
 u_i(t) &= U_i^o \text{ (unlocked), for } e_i^U(t) < 0 \text{ or } e_i^L(t) > 0
 \end{aligned}
 \tag{1}$$

The range through which the actuating error signal varies before the switching occurs is called a differential gap. By limiting the amplitude of the differential gap, one obtains a system with less oscillations. In this numerical simulation, the differential gap is related to the size of the implemented time step. The time history of the strain in a controlled SE wire is illustrated in Figure 14(b).

Analyzing the plots in Figure 15, one can see that the semi-active system is able to bound the strains in the SE wires between an upper and a lower strain limit, which, for this case study, are set to 3.0% and zero, respectively. When, during the dynamic oscillations, the strain in a given wire reaches one of these values, the corresponding support is unlocked until the mass displacement is reversed.

The process of unlocking and subsequent locking of a SE wires allows the system either to increase their cumulative strain, when compensating for excessively low strains, or to decrease them, when compensating for excessively high strains. As the compensation for lower strains is larger and usually more frequent than the compensation for higher strains, the final accumulated strain in the SE wires is positive. For the current case study the final accumulated strain in the system adds up to about 1.5%. Note that, there is no need for additional energy input to enforce the strain the SE wires, as the system uses the energy of the excitation itself. As the dynamic displacements develop, the system uses them to gradually increase the strain in the SE wires, inside the established PEW. When a wire is unlocked, the system's stiffness decreases momentarily, leading to slighter higher displacements amplitudes when compared with it's pre-strained counterpart. By limiting the strains, the system might also limit the martensite

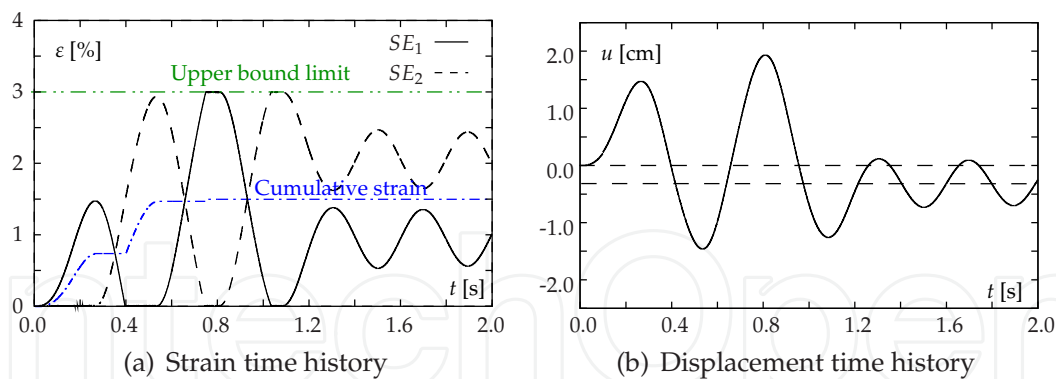


Fig. 15. Semi-active system subjected to a harmonic load

transformation ratio in the SE wires (in this test  $\zeta_{max} = 30\%$ ) and, hence, the amount of energy dissipated per time. When this happens, the system takes longer to attain the steady state free vibration phase. However, the oscillations amplitude in this last stage is of the same order of magnitude as in the pre-strained system, see Figures 13(b) and 15(b).

To emphasize its reliability, the semi-active system is excited next with a similar harmonic ground acceleration, of doubled amplitude,  $2.5 \text{ ms}^{-2}$ . To obtain a clearer picture of the steady state forced vibration phase, the duration of the excitation was also incremented from 1 to 3 seconds. The results of the numerical simulation presented in Figure 16 show that, although the displacements exhibited by the system increase accordingly, the strains in the SE wires continue to be bounded by the defined strain limits. The stress-strain hysteretic cycles presented in Figures 16(c) and 16(d) for the two SE wires show that, as a natural consequence of the applied strain constraints, the stresses in the corresponding SE wires are bounded as well. It is known that the stress levels, related to the beginning and ending of the forward and inverse transformations, are temperature dependent. For this particular loading frequency, during the initial mechanical loading cycles, the mean temperature of the SE wires decreases, until it stabilizes around a certain value. This phenomenon causes, during this transitional phase, a decrease of the stress upper bound limit for both SE wires. This phenomena can be observed in Figure 16(e), side by side with the system's force-displacement response curve, Figure 16(f).

As already mentioned, the original passive system that served as starting point for the present proposal of a semi-active system, has no recentering capability, a mandatory feature for seismic applications. To accomplish this requirement, a third restoring element is usually introduced (Dolce et al., 2000; 2005). This element enhances the recentering capability of the system, driving it back towards its original equilibrium position. Assuming it has a pure elastic behavior, the force it delivers is proportional to the final displacement of the system. It is the balance between this force and the total stiffness of the two sets of SE wires when the system drifts away from its final equilibrium position, that defines the final equilibrium position of the system. This element can have a simple elastic behavior or it can also be a SE wire, further increasing the damping capabilities of the system. In the proposed semi-active control device the recentering capabilities can, under certain conditions, be assured by its ability to control the displacements of the wires at their supports. To emphasize this aspect, one considers again

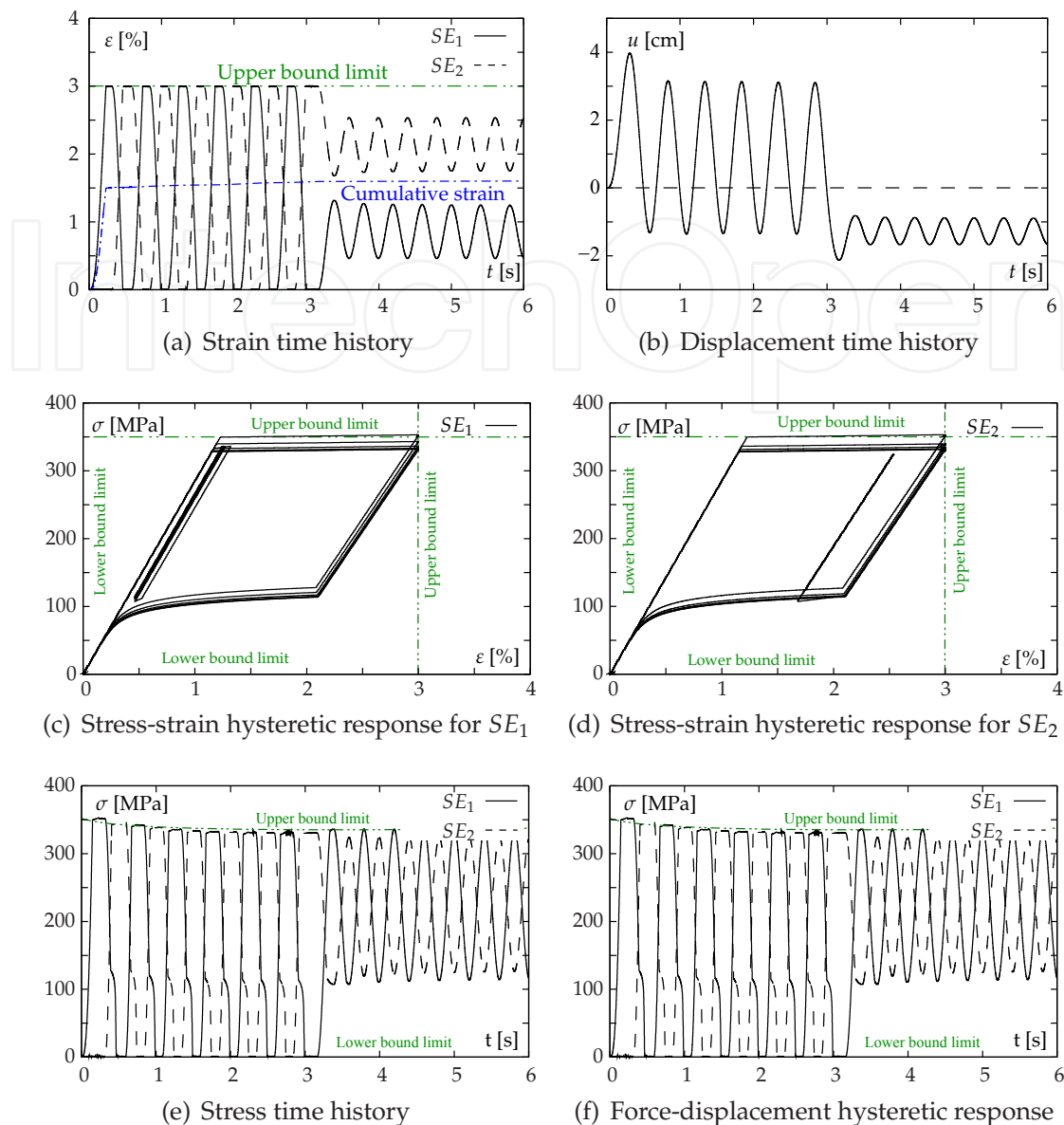


Fig. 16. Semi-active system subjected to an harmonic load of higher amplitude

the 1 second, 2 Hz harmonic ground acceleration with an amplitude of  $1.25 \text{ ms}^{-2}$  and focus on the response of the proposed device, once it reaches its steady state free vibration phase. Analyzing the displacement time history in Figure 17(b), one can see that, at the end of the loading period, the system oscillates around a new equilibrium position. To recover the initial equilibrium position, the strains/stresses in the SE wires are gradually set free, by unlocking the wires supports. During this process, the hysteretic loop is closed and the energy accumulated during straining is set free. This gives the system an extra damping capability that enables it to further decrease the amplitude of the free oscillations.

However, if the displacements amplitude exceeds a certain, pre-defined level during the loading period, the releasing of the strain/stress in the SE wires might not imply recovering of

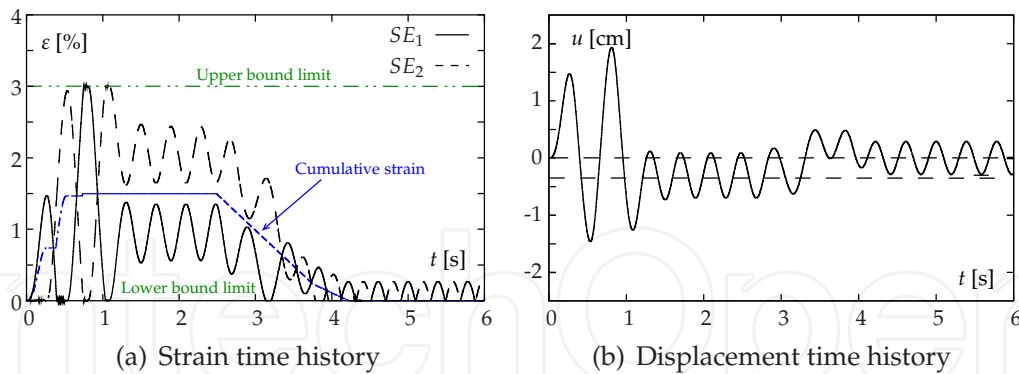


Fig. 17. recentering of the semi-active system subjected to an harmonic load

the initial equilibrium position. To regain the system recentering capability, a third elastic element should be used. To illustrate this situation, the relative displacements with respect to their initial positions, of two markers,  $M_1$  and  $M_2$ , situated on the SE wires adjacent to the corresponding supports, see Figure 11(b), are plotted in Figure 18 for three different loading cases. The first graph, Figure 18(a), corresponds to the loading case that produces the dynamic

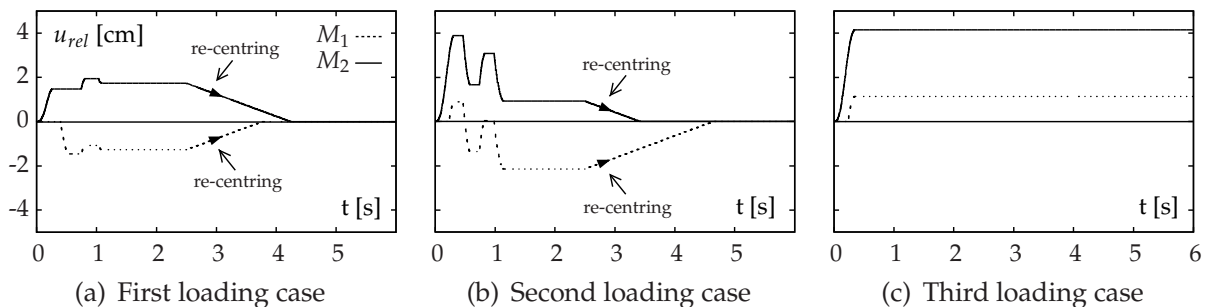


Fig. 18. Relative displacements of the SE wires at the supports.

response presented in Figure 17. One can see that, throughout most of the test,  $M_1$  and  $M_2$  move downwards and upwards, respectively, as the wires are released to compensate for low strains. When high strains are needed to be compensated,  $M_1$  and  $M_2$  reverse their movement but remain, however positive and negative, respectively. During the steady state free vibration phase, if the system releases the wires until  $M_1$  and  $M_2$  reach their initial position, the system is able to re-position itself in the original position, as already shown in Figure 17(b). In the second loading case, when the amplitude of the dynamic loading is doubled, while compensating for high strains, situations occur where  $M_1$  becomes positive, as illustrated in Figure 18(b). However, as the system reaches its steady state free vibration phase with  $M_1$  negative and  $M_2$  positive, is still able to re-position itself. This is no longer the case if, with a different duration of the load, the system reaches its steady state free vibration phase in a situation where both  $M_1$  and  $M_2$  are positive, see Figure 18(c). From this configuration it is impossible to recover the original system position by just releasing the wires. This action will only cause further displacements in the positive direction of marker  $M_1$ . Therefore, one can

conclude that, for similar situations, when the amplitude of the oscillations exceeds a pre-defined value, the system might lose its recentering capabilities. If one wants to guarantee the recentering capabilities for virtually any loading, a third elastic element should be used in the system, as in the case of passive control devices (Dolce et al., 2000; 2005).

### 4.3.1 Functioning of the proposed semi-active system

To better explain the sequence of actions taken by the proposed semi-active system during a dynamic excitation, one considers a typical displacement time-history response to an harmonic excitation, see Figure 19.

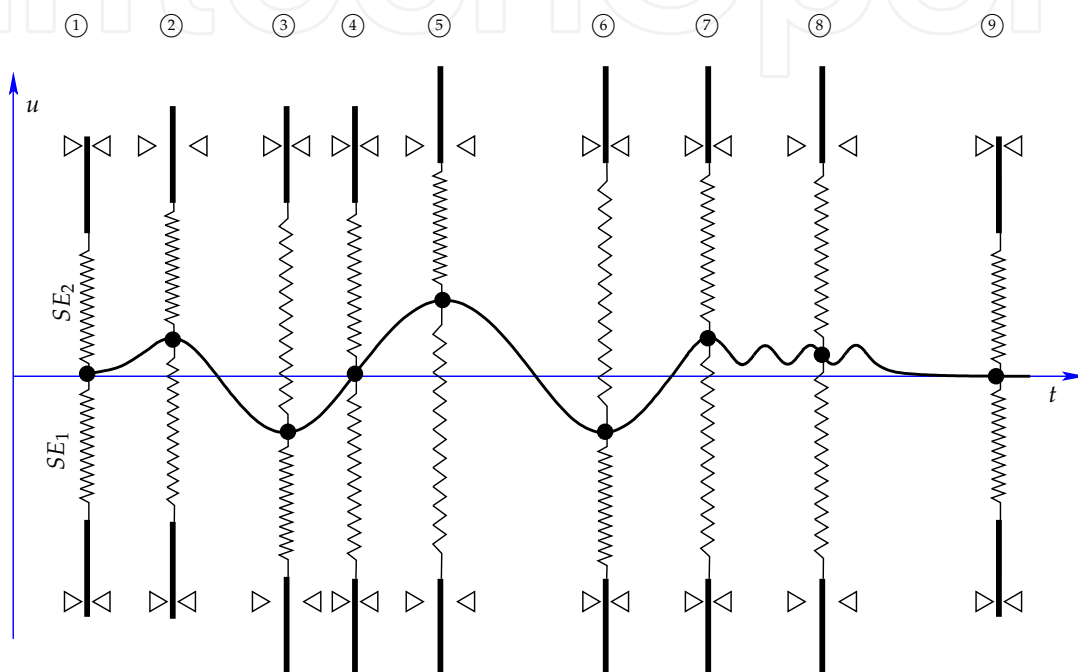


Fig. 19. Functioning of the proposed semi-active control system

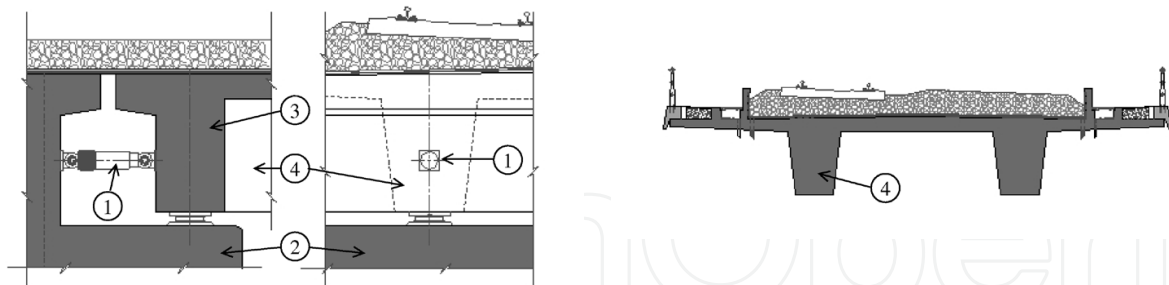
The analysis starts with the system resting in its original equilibrium position, referred as position ① in the graph. In this position both of the SE wires,  $SE_1$  and  $SE_2$ , are strain/stress free and their supports,  $S_1$  and  $S_2$ , are locked. Once the harmonic excitation is applied to the system, the mass starts to move (assume) upwards and the straining of  $SE_1$  begins. During the first half cycle of the movement, between position ① and ②,  $S_2$  is unlocked to prevent compression in the corresponding wire, while the support of  $SE_1$  is kept locked, to ensure the straining of the wire. As the mass reverses its direction,  $S_2$  switches to locked, to preserve the accumulated strain in the wire. As the movement continues downwards, the support of  $SE_1$  remains locked as well, until the mass reaches its original equilibrium position. With this configuration, displacements below this point would cause compression in the  $SE_1$ . For this reason, as soon as this happens,  $S_1$  switches to unlocked, until position ③, when the mass reverses once again its direction. At the end of the first loading cycle, position ④, both SE wires have already accumulated a certain level of strain. Note that this strain was introduced in the system by the external dynamic load itself, without any need of supplemental energy input. Between positions ④ and ⑤, assuming that in the last one occurs the maximum displacement amplitude, both supports will switch from locked to unlocked:  $S_2$ , as the strain

in  $SE_2$  approaches zero to avoid compression, and  $S_1$ , as the strain in  $SE_1$  goes beyond the defined value inside the PEW, preventing it from further straining. If, during an eventual steady state forced vibration phase, positions ⑤ to ⑥, there is no need for adjustments in the SE wires to compensate low or high strains, both supports remain locked. As soon as the dynamic excitation ceases, position ⑦, the amplitude of the free vibrations starts gradually to diminish because of the SE damping. The system reaches its steady state free vibration phase, position ⑧, oscillating around an equilibrium position different from its original one. During this period, both supports remain locked. At this point, to recover the original equilibrium position, the system unlocks both of the cables, relinquishing the accumulated strain in the wires. Finally, position ⑨, the supports are locked again to prepare the device for the next dynamic excitation.

Note that, every time the system needs to unlock a support, the wire is released with a controlled velocity, which can be seen as a design parameter of the proposed semi-active device. In all the harmonic tests reported here, this velocity was set to 0.6 m/s.

## 5. Proposed semi-active vibration control device under seismic excitation

Studies on the efficiency of SMA based passive control devices in the context of seismic loading were reported in (Cismasiu & Santos, 2008), considering a simplified numerical model of the São Martinho railway viaduct, see Figure 20. This pre-stressed concrete structure, with a total length, between abutments, of 852.0 m, is built up of seven, 113.6 m length, independent segments and one segment of 56.8 m, adjacent to the south abutment. These segments are divided into 28.4 m spans and are structurally independent. The railway deck is a 13.0 m wide beam slab, comprising two  $2.0 \times 1.4$  m main girders. The foundations are materialized by 1.2 m diameter piles with an average length of about 30.0 m. The concrete piers are tubular and have an average height of 12.0 m. Each pier is supported by five piles.



Legend: 1. Control device, 2. Abutment, 3. Transverse girder, 4. Main girder

Fig. 20. São Martinho railway viaduct: Control device location and mid-span cross section

For the longitudinal analysis of the viaduct, it is assimilated to an elastic, one degree-of-freedom dynamic system, with 4650 ton mass and a stiffness of  $355 \times 10^3$  kN/m, having a structural damping of 5%. The records of two historic strong earthquakes, *El Centro*, with a magnitude of  $7 M_W$  and *Kobe*, with a magnitude of  $6.9 M_W$ , as provided by the Pacific Earthquake Engineering Research Center and the University of California in the PEER Strong Motion Database (Pac, <http://peer.berkeley.edu/smcat>), are used in the numerical simulation.

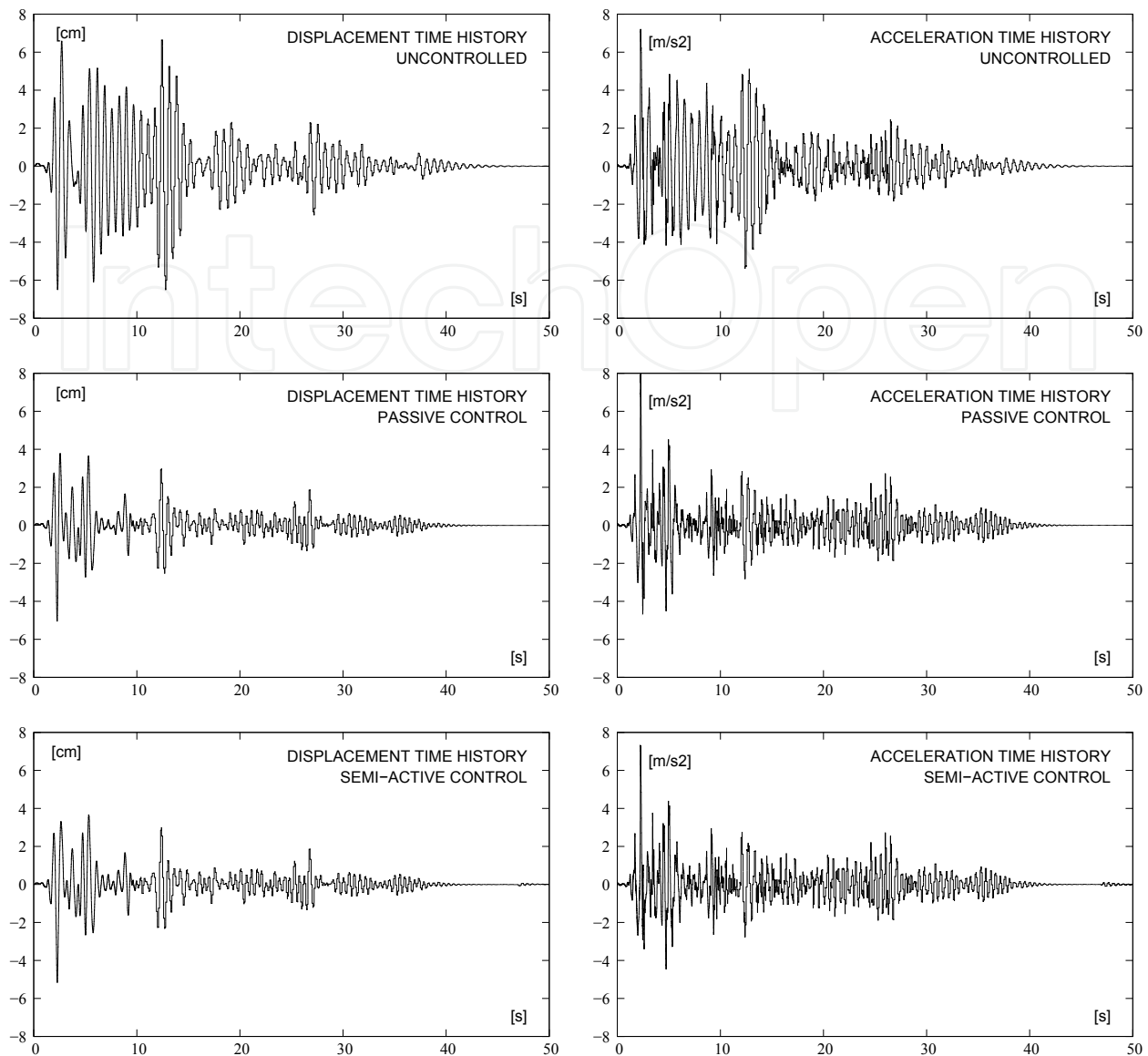


Fig. 21. Response of the structure to the *El Centro* earthquake: displacement and acceleration time history for the free and controlled structure.

To emphasize the benefits of the proposed semi-active control device on the structural response of the structure, three cases are considered: the uncontrolled structure, the structure controlled with a SMA based passive device and the structure controlled with the semi-active device. Note that, in order to get comparable sets of results, the strain level in the SE wires of the passive device was set equal with the maximum strain level attained in the semi-active device. To obtain an adequate response of the semi-active device to the higher frequency content of the seismic action, when the supports are unlocked, the wires are released with a velocity of 1 m/s. Two control devices, both either passive either semi-active, are placed at one end of the viaduct, one for each main girder. Each of them is composed of two sets of 1.0 m SMA wires, each set with a total area of 100 cm<sup>2</sup>. This section could be built up of bars or a set of smaller wires laid parallel in strands, to form a cable. The mechanical characteristics of the SMAs are the ones defined in Table 1. A pre-strain of 2.25 % is considered in the passive

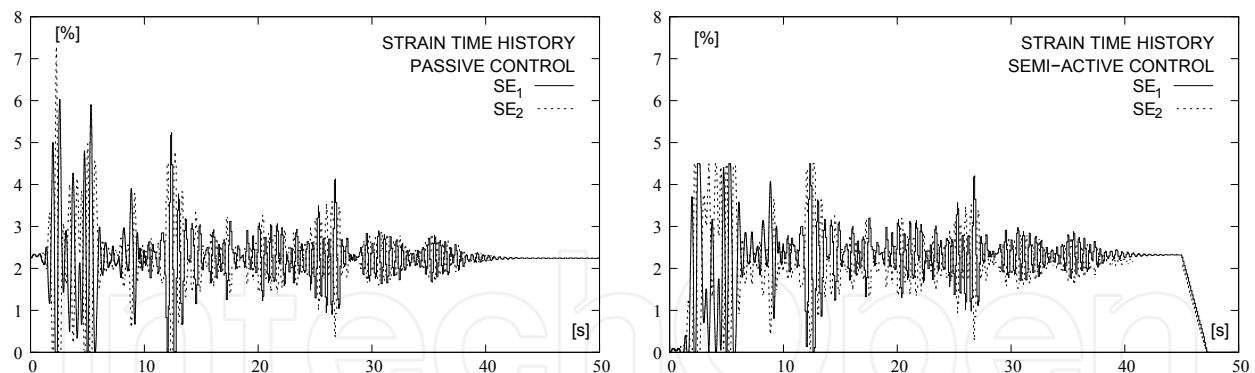


Fig. 22. Response of the structure to the *El Centro* earthquake: strain time history in the SE wires of the controlled structure.

device, equal to the resulting cumulative strain in the semi-active device. The displacement and acceleration time histories of the viaduct deck in the longitudinal direction, as well as the strain time history in the SE wires of the passive and semi-active control system, obtained when the structure was subjected to *El Centro* earthquake, are presented in Figures 21 and 22, respectively.

Analyzing the plots in Figure 21, one can see that, during the seismic excitation, the two control devices exhibit similar damping characteristics, being able to considerably reduce the amplitude of the earthquake induced displacements and accelerations. The plots in Figure 22 however, illustrate that the strain time history in the SE wires is quite different for the two adopted control solutions. Although the pre-strain in the passive device is equal to the cumulative strain in the semi-active device, one can see that the maximum strains developed in the passive device are considerably larger when compared with the ones developed in its semi-active counterpart. As their values are outside the PEW, the long term behavior of the passive device might be compromised. However, no failure occurs in the SE wires during the earthquake. One can observe that, when the seismic excitation stops, the SE wires return to their initial pre-strain, favoring the occurrence of relaxation phenomena. On the other hand, in the semi-active device, the wires return to their strain free condition at the end of the loading.

To conclude, one may say that, for the given seismic excitation, except for the long term relaxation phenomena, the two control solution produce equivalent results. One must note, however, that the pre-strain level in the passive control device was calibrated according to the given seismic excitation, in order to avoid failure in the SE wires. If a different seismic action is applied to the same structure configuration, the results might be completely different. In order to illustrate this behavior, the structure is subjected next to the *Kobe* earthquake.

Analyzing the dynamical response of the structure presented in Figures 23 and 24, one can see that the passive control device fails, as its SE wires' ultimate strain capacity ( $\simeq 10 - 12\%$ ) is exceeded. Besides relaxation and creep potential problems, the fact that this type of solutions need an *a priori* value for the level of pre-strain in the SE wires, represent an important drawback in the case of seismic applications. While estimates for the maximum strain in the SE wires are relatively easy to obtain in the case of service loads, and therefore a corresponding

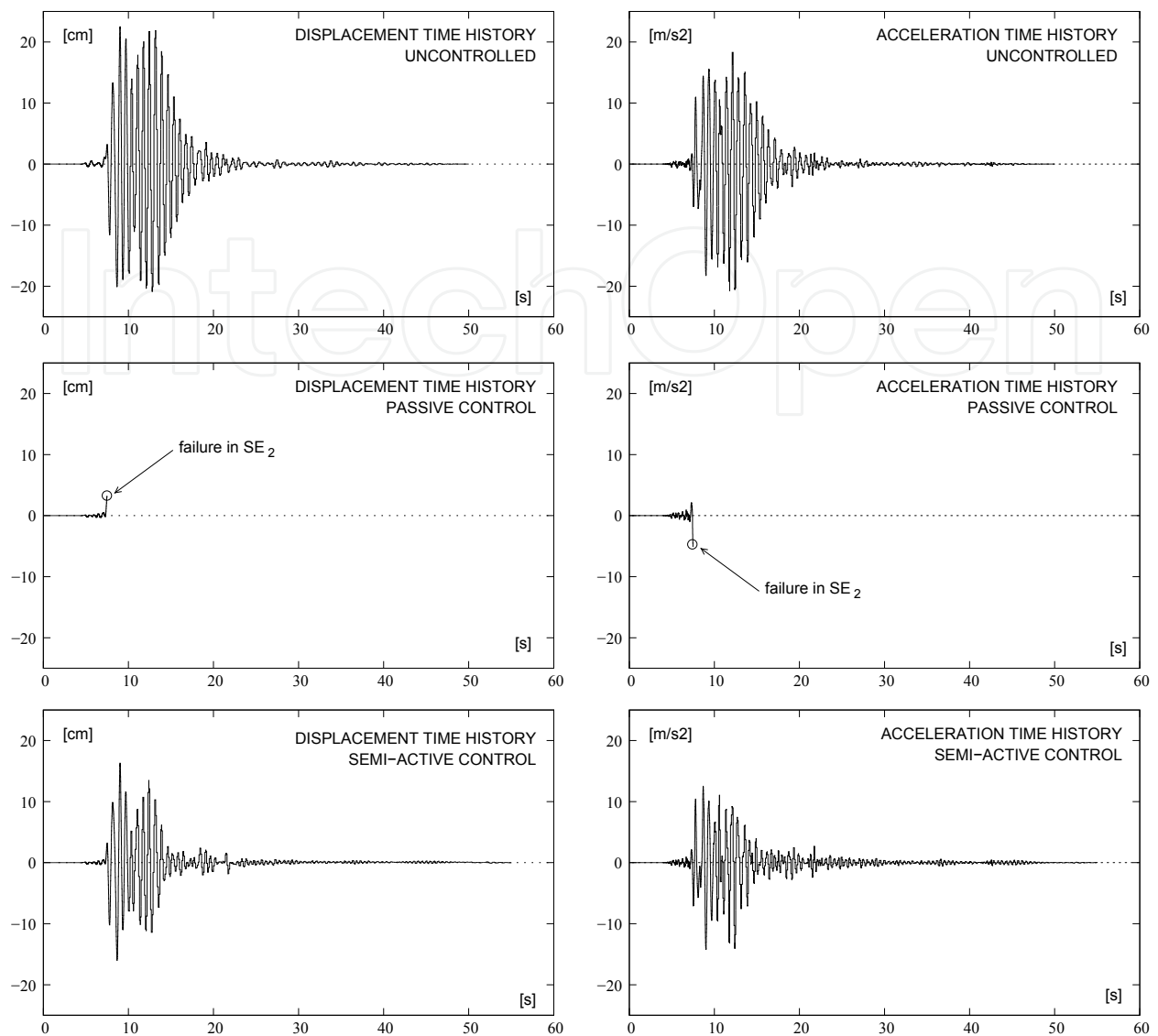


Fig. 23. Response of the structure to the *Kobe* earthquake: displacement and acceleration time history for the free and controlled structure.

value for the necessarily pre-strain can be computed, this is no longer the case for extraordinary dynamic loads.

With no need of initial pre-strain calibration, its semi-active counterpart responds well to virtually any level of dynamic excitation, as illustrated here in the case of the *Kobe* earthquake. When the response of the structure is compared with the one obtained for the *El Centro* earthquake, one can see that the system exhibits similar characteristics. It presents important damping capabilities, is able to confine the strains in the SE wires to predefined levels, inside the PEW, and finally, at the end of the action, is able to recover the SE wires strain free condition.

Another benefic aspect related to the semi-active control device is its ability to confine the force values throughout the entire duration of the seismic action, meaning that, when implemented in a civil engineering structure, the force the semi-active device transmits to the structure

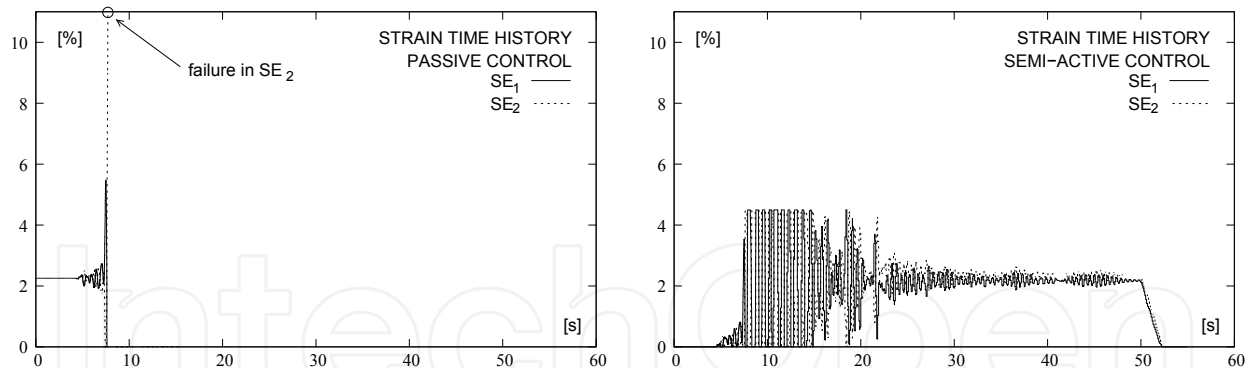


Fig. 24. Response of the structure to the *Kobe* earthquake: strain time history in the SE wires of the controlled structure.

can be conveniently bounded. This feature is very important in the designing process of the structure itself.

## 6. Conclusions

The proposed semi-active vibration control device originates from a passive control system, based on SE austenitic wires. In its semi-active version, the system monitors the feedback measurements and based on this information, continuously adjust the strain in the SE wires in order to improve its dynamical characteristics.

The strain accumulation in the wires is a result of the motion of the structure itself, with no need of external energy input in the system. To avoid relaxation phenomena, the SE wires are set strain free at the end of the loading period.

The system is able to dissipate a considerable amount of energy, while keeping the SE wires inside the recoverable limits defined by the PEW, to minimize the rheological effects related to cumulative creep. It also guarantees a minimal threshold to the strain level in the SE wires to avoid compression and exhibit efficient recentering capabilities.

The reported numerical simulations clearly demonstrate the potential the proposed semi-active control device has, in improving the seismic response of civil engineering structures. These results are expected to be confirmed with experimental tests in the near future, as a small scale prototype of the device is currently being developed.

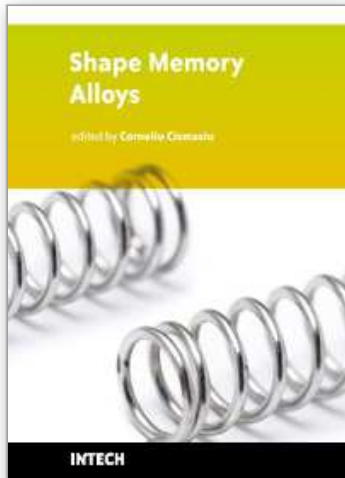
## 7. Acknowledgment

This work is part of the research developed in UNIC, the Research Center of the Department of Civil Engineering, Faculty of Science and Technology of the Nova University of Lisbon and partially supported by contract SFRH/BD/37653/2007 with Fundação para a Ciência e Tecnologia. Cooperation with Professor F. M. Braz Fernandes from CENIMAT, the Center of Materials Research of the same institution is gratefully acknowledged.

## 8. References

- Auguet, C., Isalgue, A., Torra, V., Lovey, F. & Pelegrina, J. (2008). Metastable effects on martensitic transformation in SMA. Aging problems in NiTi, *Journal of Thermal Analysis and Calorimetry* **92**(1): 63–71.
- Auricchio, F., Fugazza, D. & DesRoches, R. (2006). Numerical and experimental evaluation of the damping properties of shape-memory alloys, *Journal of Engineering Materials and Technology* **128**(3): 312–319.
- Auricchio, F. & Sacco, E. (1997). A one-dimensional model for superelastic shape-memory alloys with different elastic properties between austenite and martensite, *International Journal of Non-Linear Mechanics* **32**(6): 1101–1114.
- Auricchio, F., Taylor, R. L. & Lubliner, J. (1997). Shape-memory alloys: macromodelling and numerical simulations of the superelastic behaviour, *Computer Methods in Applied Mechanics and Engineering* **146**: 281–312.
- Bhattacharyya, A., Sweeney, L. & G., F. M. (2002). Experimental characterization of free convection during thermal phase transformations in shape memory alloy wires, *Smart Material and Structures* **11**: 411–422.
- Brinson, L. C. & Huang, M. S. (1996). Simplifications and comparisons of shape memory alloy constitutive models, *Journal of Intelligent Material Systems and Structures* **7**: 108–114.
- Chopra, A. K. (2001). *Dynamics of Structures: theory and applications to earthquake engineering*, 2<sup>nd</sup> edn, Prentice-Hall, Inc., Upper Saddle River, NJ 07458.
- Cismasiu, C. & Santos, F. P. A. (2008). Numerical simulation of superelastic shape memory alloys subjected to dynamic loads, *Smart Materials and Structures* **17**(2): 25–36.
- Collings, E. W. (1995). *Materials Properties Handbook: Titanium Alloys*, ASM International.
- DesRoches, R. & Delemont, M. (2002). Seismic retrofit of simply supported bridges using shape memory alloys, *Engineering Structures* **24**: 325–332.
- Dolce, M., Cardone, D. & Marnetto, R. (2000). Implementation and testing of passive control devices based on shape memory alloys, *Earthquake Engineering and Structural Dynamics* **29**: 945–968.
- Dolce, M., Cardone, D., Ponzo, F. C. & Valente, C. (2005). Shaking table tests on reinforced concrete frames without and with passive control systems, *Earthquake Engineering and Structural Dynamics* **34**: 1687–1717.
- Höhne, G., Hemminger, W. F. & Flammersheim, H.-J. (2003). *Differential Scanning Calorimetry*, 2<sup>nd</sup> edn, Springer.
- Holman, J. (2009). *Heat Transfer*, McGraw-Hill Series in Mechanical Engineering, McGraw-Hill Science/Engineering/Math.
- Housner, G. W., Bergman, L. A., Caughey, T. K., Chassiakos, A. G., Claus, R. O., Masri, S. F., Skelton, R. E., Soong, T. T., Spencer, B. F. & Yao, J. T. P. (1997). Structural control. Past, present, and future, *Journal of Engineering Mechanics* **123**(9): 897 – 971.
- Isalgue, A., Torra, V., Yawny, A. & Lovey, F. C. (2008). Metastable effects on martensitic transformation in SMA. Part VI. The Clausius-Clapeyron relationship, *Journal of Thermal Analysis and Calorimetry* **91**(3): 991–998.
- Ivshin, Y. & Pence, T. J. (1994). A thermomechanical model for a one variant shape memory material, *Journal of Intelligent Material Systems and Structures* **5**(4): 455–473.
- Jones, D. R. H. & Ashby, M. F. (1998). *Engineering Materials: An Introduction to Microstructures, Processing and Design*, Vol. 2 of *International Series on Materials Science and Technology*, 2<sup>nd</sup> edn, Butterworth-Heinemann.

- Koistinen, D. P. & Marburger, R. E. (1959). A general equation prescribing the extent of the austenite-martensite transformation in pure iron-carbon alloys and plain carbon steels, *Acta Metall* **7**: 59–60.
- Liang, C. & Rogers, C. A. (1990). One-dimensional thermomechanical constitutive relations for shape memory materials, *Journal of Intelligent Systems and Structures* **1**: 207–234.
- Magee, C. L. (1970). Nucleation of martensite, *Phase Transformations*, ASM pp. 115–156.
- Matsui, R., Tobushi, H. & Ikawa, T. (2004). Transformation-induced creep and stress relaxation of TiNi shape memory alloy, *Proceedings of the Institution of Mechanical Engineers, Part L: Journal of Materials: Design and Applications* **218**(4): 343–353.
- McCormick, J., DesRoches, R., Fugazza, D. & Auricchio, F. (2006). Seismic vibration control using superelastic shape memory alloys, *Journal of Engineering Materials and Technology* **128**(3): 294–301.
- Miyazaki, S., Imai, T. & Otsuka, K. (1986). Effect of cyclic deformation on the pseudoelasticity characteristics of Ti-Ni alloys, *Metalurgical Transactions A* **17A**: 115.
- Moumni, Z., Van Herpen, A. & Riberty, P. (2005). Fatigue analysis of shape memory alloys: energy approach, *Smart Materials and Structures* **14**: 287–292.
- Ocel, J., DesRoches, R., Leon, R. T., Hess, W. G., Krumme, R., Hayes, J. R. & Sweeney, S. (2004). Steel beam-column connections using shape memory alloys, *Journal of Structural Engineering* **130**(5): 732–740.
- Ortín, J. & Delaey, L. (2002). Hysteresis in shape-memory alloys, *International Journal of Non-Linear Mechanics* **37**: 1275–1281.
- Otsuka, K. & Wayman, C. M. (eds) (1998). *Shape memory materials*, Cambridge University Press.
- Pac (<http://peer.berkeley.edu/smcat>). *PEER Strong Motion Database*.
- Shook, D. A., Roschke, P. N. & Ozbulut, O. E. (2008). Superelastic semi-active damping of a base-isolated structure, *Structural Control and Health Monitorig* **15**: 746–768.
- Symans, M. D. & Constantinou, M. C. (1999). Semi-active control systems for seismic protection of structures: a state-of-the-art review, *Engineering Structures* **21**: 469–487.
- Tanaka, K., Kobayashi, S. & Sato, Y. (1986). Thermomechanics of transformation pseudoelasticity and shape memory effect in alloys, *International Journal of Plasticity* **2**: 59–72.
- Torra, V., Isalgue, A., Martorell, F., Terriault, P. & Lovey, F. (2007). Built in dampers for family homes via SMA: An ANSYS computation scheme based on mesoscopic and microscopic experimental analyses, *Engineering Structures* **29**: 1889–1902.
- Vitiello, A., Giorleo, G. & Morace, R. E. (2005). Analysis of thermomechanical behaviour of Nitinol wires with high strain rates, *Smart Material and Structures* **14**: 215–221.
- Zhang, Y. & Zu, S. (2007). A shape memory alloy-based reusable hysteretic damper for seismic hazard mitigation, *Smart Materials and Structures* **16**: 1603–1623.



## **Shape Memory Alloys**

Edited by Corneliu Cismasiu

ISBN 978-953-307-106-0

Hard cover, 210 pages

**Publisher** Sciyo

**Published online** 18, October, 2010

**Published in print edition** October, 2010

In the last decades, the Shape Memory Alloys, with their peculiar thermo-mechanical properties, high corrosion and extraordinary fatigue resistance, have become more popular in research and engineering applications. This book contains a number of relevant international contributions related to their properties, constitutive models and numerical simulation, medical and civil engineering applications, as well as aspects related to their processing.

### **How to reference**

In order to correctly reference this scholarly work, feel free to copy and paste the following:

Corneliu Cismasiu and Filipe P. Amarante Dos Santos (2010). Numerical Simulation of a Semi-Active Vibration Control Device Based on Superelastic Shape Memory Alloy Wires, Shape Memory Alloys, Corneliu Cismasiu (Ed.), ISBN: 978-953-307-106-0, InTech, Available from: <http://www.intechopen.com/books/shape-memory-alloys/numerical-simulation-of-a-semi-active-vibration-control-device-based-on-superelastic-shape-memory-al>

**INTECH**  
open science | open minds

### **InTech Europe**

University Campus STeP Ri  
Slavka Krautzeka 83/A  
51000 Rijeka, Croatia  
Phone: +385 (51) 770 447  
Fax: +385 (51) 686 166  
[www.intechopen.com](http://www.intechopen.com)

### **InTech China**

Unit 405, Office Block, Hotel Equatorial Shanghai  
No.65, Yan An Road (West), Shanghai, 200040, China  
中国上海市延安西路65号上海国际贵都大饭店办公楼405单元  
Phone: +86-21-62489820  
Fax: +86-21-62489821

© 2010 The Author(s). Licensee IntechOpen. This chapter is distributed under the terms of the [Creative Commons Attribution-NonCommercial-ShareAlike-3.0 License](#), which permits use, distribution and reproduction for non-commercial purposes, provided the original is properly cited and derivative works building on this content are distributed under the same license.

IntechOpen

IntechOpen